

# Synthesis and Phase Transitional Behavior of Dimer-like Optically Active Liquid Crystals

Govindaswamy Shanker<sup>†</sup> and Channabasaveshwar V. Yelamaggad\*

Centre for Soft Matter Research, Prof. U. R. Rao Road, P. B. No. 1329, Jalahalli, Bangalore 560 013, India

 Supporting Information

**ABSTRACT:** The results of our detailed studies pertaining to a relatively new class of low molar mass mesogens are presented. Four homologous series of optically active dimer-like mesogens, comprising cholesterol as the conventional pro-mesogenic core covalently tethered to a nonmesogenic salicylaldimine segment through a flexible spacer of varying length and parity, have been synthesized and evaluated for their thermal, electrical switching, electrochemical, and gelation properties. The thermal behavior, being the prime focus of this study, has been characterized by optical, calorimetric, X-ray diffraction, and electrical switching studies. In each series, the length of the even/odd-parity spacer is held constant, while the length of the terminal *N*-alkyl tail attached to nonmesogenic salicylaldimine core has been varied to gain insight into the fundamental correlation between structure and phase transitional properties. These compounds, with a few exceptions, exhibit liquid crystal phase(s); the identified phases are chiral nematic ( $N^*$ ), twist grain boundary (TGB), chiral smectic A (SmA), and chiral smectic C (SmC\*) phases. The selective reflection property of the  $N^*$  phase and ferroelectric behavior of the SmC\* phase have been ascertained for some selected members. In general, the phase behavior shows a dependence on the length and parity of the central spacer as well as the length of the terminal tail. The odd–even effect has been prominently found in the clearing temperatures; the even-parity dimer-like compounds belonging to three different series exhibit higher values when compared to members of an odd-parity series. Thus, our study demonstrates that these new class of low molar mass materials behave analogous to liquid crystal dimers. Electrochemical behavior and gelation ability have been demonstrated for some selected materials.



## I. INTRODUCTION

Liquid crystal (LC) phases, owing to their special structural features and unique properties, have been attracting a great deal of attention in both fields of basic research and practical applications.<sup>1</sup> Specifically, LC phases formed by rod-like and disk-shaped organic molecules, called conventional mesogens, have been studied intensively, and, as a result, they have been used in different technologies. However, over the years, several new mesogenic motifs differing in their shape-anisotropy from conventional LCs have been designed, prepared, and shown to exhibit mesomorphism with improved characteristics and desired functionality.<sup>2–6</sup> LC dimers, which are made by covalently tethering two identical (symmetrical) or nonidentical (non-symmetrical) conventional mesogens through a flexible spacer of varying length and parity, are among the large variety of nonconventional LCs reported hitherto.<sup>4–6</sup> These compounds, which were initially regarded as model systems for LC polymers,<sup>5a–c</sup> are of significant interest in their own right as they display different thermal behavior than conventional LCs. One of the most striking characteristics of this class of low molar mass LCs is the critical dependence of their transitional behavior on the length and parity (odd–even) of the flexible spacer.<sup>4</sup> The most immediately apparent effect is the prominent alternations in clearing temperature and associated entropy change upon varying the parity of the spacer; for example, the dimers with an

even-parity spacer exhibit higher clearing temperature than that of odd-parity members.<sup>4,5</sup>

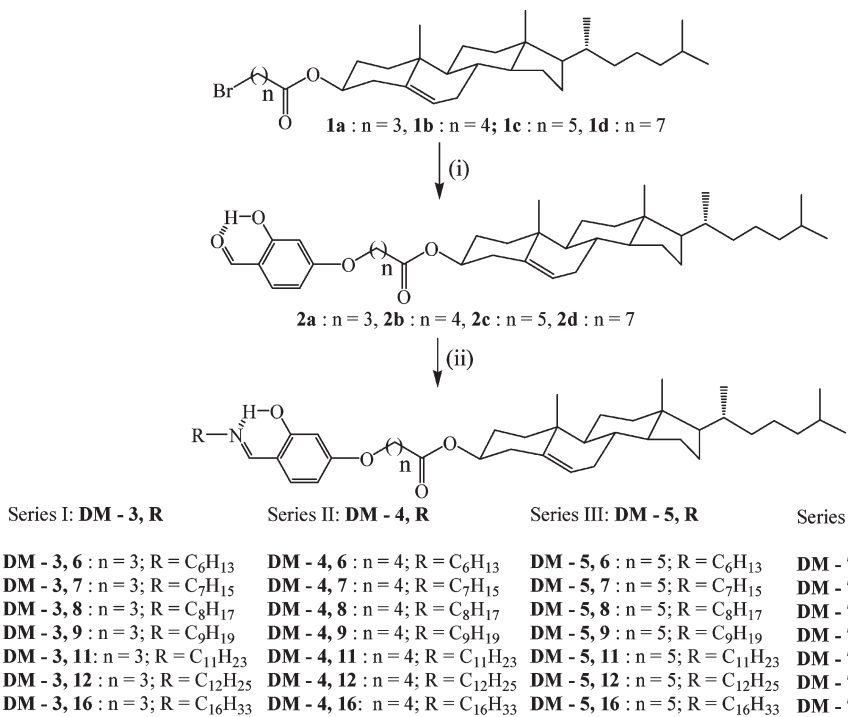
In fact, another class of low molar mass mesogens made by covalently joining a typical mesogenic (two-ring) core with a bulky nonmesogenic segment, such as one-ring aliphatic/aromatic cores, via a flexible spacer is also known since the early 1970s.<sup>4,6–20</sup> Notably, their thermal behavior closely resembles that observed in LC dimers. For example, the spacer parity drastically influences their transitional property; in particular, clearing temperatures exhibit a dramatic odd–even effect as the parity of the spacer is varied. They have been regarded as the structural intermediates between classical low molar mass mesogens (monomers) and LC dimers; thus, they can be referred to as “dimer-like” mesogens. Hitherto, several series of both achiral and chiral dimer-like mesogens have been reported, and the studies indicate their thermal behavior dependence on the chemical nature and/or size of the nonmesogenic segment attached to the conventional mesogen via a flexible spacer. The chiral dimer-like compounds, formed by tethering cholesterol and benzene core (with or without substitution) via a spacer, especially attracted our attention as they display monotropic

**Received:** July 1, 2011

**Revised:** August 5, 2011

**Published:** August 10, 2011

Scheme 1



Reagents and conditions (i) 2,4-Dihydroxybenzaldehyde, anhyd. K<sub>2</sub>CO<sub>3</sub>, butanone, reflux, 12 h (78–85%) (ii) *n*-Alkylamines, dry EtOH, AcOH (catalytic), reflux, 1 h (68–80%)

**Table 1.** Phase Transition Temperatures (°C)<sup>c</sup> and Associated Enthalpies [Jg<sup>-1</sup>]<sup>d</sup> of Dimer-like Mesogens Belonging to the DM-3,R Series<sup>a</sup>

Compound	Phase sequence	
	Heating	Cooling
DM-3,6	Cr 98.3 [32.1] N* 124.1 [2.4] I	I 123.6 [2.4] N* 97 TGB 95.5 [0.8] <sup>e</sup> SmA 57.9 [7.1] Cr
DM-3,7	Cr 104.1 [56.7] N* 114 [3.6] I	I 111.6 [3.5] N* 88.2 <sup>e</sup> TGB 86. <sup>f</sup> SmA 62.4 <sup>e</sup> SmC* 40.5 Cr <sup>g</sup>
DM-3,8	Cr 87.4 [46.8] SmA 105.1 TGB 106.9 [0.9] <sup>e</sup> N* 120.5 [2.5] I	I 119.9 [2.4] N* 106.3 TGB 104.6 [1] <sup>e</sup> SmA 71.2 <sup>f</sup> SmC* 40.8 <sup>f</sup> Cr
DM-3,9	Cr 94.3 [47.3] SmA 110.2 TGB 111.6 [0.9] <sup>e</sup> N* 121.1 [3.1] I	I 120.4 [2.8] N* 111.2 TGB 109.5 [0.8] <sup>e</sup> SmA 87.9 <sup>e</sup> SmC* 60.6 [11.9] Cr
DM-3,10 <sup>b</sup>	Cr 99.1 [46.9] SmA 111.9 TGB 113.3 [1.6] <sup>e</sup> N* 119 [3.1] I	I 118.4 [2.9] N* 112.8 TGB 111.3 [1.4] <sup>e</sup> SmA 91.1 <sup>f</sup> SmC* 58.4 [10] Cr
DM-3,11	Cr 96.5 [39.3] SmA 112.8 TGB 114.4 [2.6] <sup>e</sup> N* 118.8 [2.8] I	I 118.3 [2.6] N* 113.8 TGB 111.6 [1.3] <sup>e</sup> SmA 95.4 <sup>f</sup> SmC* 59.2 Cr <sup>g</sup>
DM-3,12	Cr 91.6 [41.2] SmA 115 [1.6] N* 116.5 [3.1] I	I 115.8 [3] N* 114.3 [1.1] SmA 89.2 <sup>f</sup> SmC* 57.9 Cr <sup>g</sup>
DM-3,16	Cr 74.3 [18.9] SmA 109.1 [4] I	I 106.2 [3.9] SmA 71.4 <sup>f</sup> SmC* 45.4 Cr <sup>g</sup>

<sup>a</sup> Cr = Crystal; SmC\* = Chiral smectic C phase; SmA = Smectic A phase; TGB = Twist grain boundary phase with either SmA or SmC blocks (SmC = Smectic C phase); TGBC\* = Twist grain boundary phase with SmC\* blocks; N\* = Chiral nematic phase; I = Isotropic phase. <sup>b</sup> Known compound but included for the sake of comparison and completeness (ref 21). <sup>c</sup> Phase transition temperatures were determined by both POM and DSC studies: peak temperatures in the DSC thermograms obtained during the first heating and cooling cycles (at 5 °C min<sup>-1</sup>) coupled with optically measured temperatures are given. <sup>d</sup> Transition enthalpies were obtained from the DSC thermograms. <sup>e</sup> Although N\*-TGB/TGB-N\* and TGB-SmA/SmA-TGB phase transitions were observed in POM, they were not resolved in DSC trace; hence the enthalpy value represents the combined enthalpy for N\*-TGB/TGB-N\* and TGB-SmA/SmA-TGB transitions. <sup>f</sup> Phase transition was observed under POM; too weak to be detected by DSC. <sup>g</sup> Crystallization was observed under POM only.

mesophase/s with a strong to moderate odd–even effect in the clearing temperatures. This is notable given the fact that they possess pro-mesogenic cholesterol and moreover, the analogous LC dimers, as demonstrated by the pioneering work of Jin and co-workers<sup>6</sup> as well as other groups,<sup>5d</sup> exhibit fascinating phase transitional behavior, with the mesophase being generally enantiotropic in nature. However, we recently observed that four dimer-like mesogens formed by covalently linking the

pro-mesogenic cholesterol entity with the *N*-(*n*-decyl)salicylaldimine core through either an even-parity or an odd-parity spacer exhibit enantiotropic mesomorphism convincingly;<sup>21</sup> this behavior can be attributed primarily to the presence of a *N*-(*n*-decyl)-salicylaldimine core that enhances the shape-anisotropy, reduces the melting point and maximizes the probability of mesophase formation. These observations inspired us to prepare the lower and higher homologues of the four mesogens mentioned above.

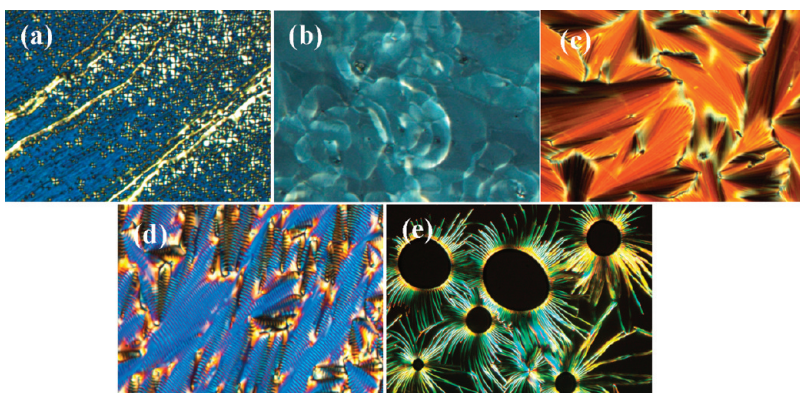


**Figure 1.** Photomicrographs of the textures observed for different mesophase of DM-3,8: (a) planar textures of the  $N^*$  phase ( $110\text{ }^\circ\text{C}$ ), (b) greyish planar texture of the TGB phase ( $105.5\text{ }^\circ\text{C}$ ), (c) focal-conic texture observed for the homogeneously aligned SmA phase ( $80\text{ }^\circ\text{C}$ ), (d) focal conics with striations seen for the homogeneously aligned SmC\* phase ( $68\text{ }^\circ\text{C}$ ), and (e) filamentary texture seen for the homeotropically aligned TGB phase ( $105\text{ }^\circ\text{C}$ ).

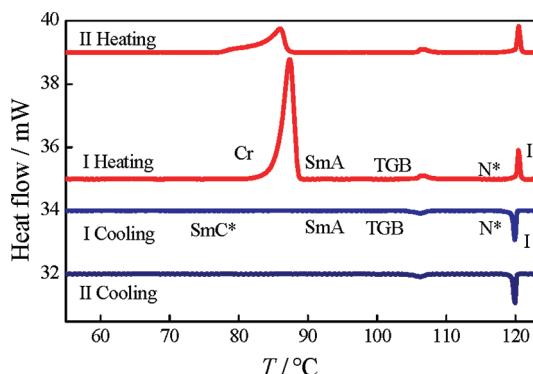


**Figure 2.** DSC thermograms of the first and second heating/cooling cycles recorded at a rate of  $5\text{ }^\circ\text{C}/\text{min}$  for the compound DM-3,8.

Herein, we report the synthesis and characterization of four series of dimer-like mesogens where the pro-mesogenic cholesterol segment covalently combines with  $N$ -(*n*-alkyl)salicylaldimine through a flexible spacer. These four series of compounds, namely, cholesteryl  $\omega$ -(3-hydroxy-4-(*n*-alkyliminomethyl)phenoxy)alkanoates, primarily differ in the number of carbon atoms of the spacer; they comprise 4-oxybutanoyloxy ( $C_4$ ; even-parity), 5-oxypentanoyloxy ( $C_5$ ; odd-parity), 6-oxyhexanoyloxy ( $C_6$ ; even-parity), and 8-oxyoctanoyloxy ( $C_8$ ; even-parity) spacers. In each series, the number of carbon atoms in the terminal tail attached to the salicylideneamine core have been varied from  $C_6$  (*n*-hexyl) to  $C_{12}$  (*n*-dodecyl); this includes the  $C_{16}$  (*n*-hexadecyl) tail also. For convenience, we denote these four series (I to IV) of compounds by mnemonics DM-3,R, DM-4,R, DM-5,R, and DM-7,R, where DM stands for Dimer-like Mesogens, and R indicates the length of the terminal *n*-alkyl tail.

## II. RESULTS AND DISCUSSION

**II.a. Synthesis and Molecular Structural Characterization.** The new dimer-like compounds belonging to series (I–IV) DM-3,R, DM-4,R, DM-5,R, and DM-7,R were prepared by synthetic steps identical to those reported earlier as shown in Scheme 1.<sup>21</sup> Cholesteryl  $\omega$ -bromoalkanoates **1a–d**, readily prepared by known methods starting from commercially available cholesterol,<sup>22</sup>

were reacted with 2,4-dihydroxybenzaldehyde in the presence of a mild base in butanone to obtain cholesteryl  $\omega$ -(3-hydroxy-4-formylphenoxy)alkanoates (**2a–d**). The acid catalyzed condensation of the salicylaldehydes **2a–d** with *n*-alkylamines in refluxing ethanol gave the target molecules in reasonably good yields. The detailed synthetic procedures and molecular structural characterization data of all the compounds are given in the Supporting Information under the heading Experimental Section.

**II.b. Evaluation of Thermal Behavior.** The phase transitional behavior of the four series of dimer-like mesogens was established with the help of a polarizing optical microscope (POM), differential scanning calorimeter (DSC), and X-ray diffraction (XRD). Clean glass slides were used to examine the LC (the birefringence and fluidity) property of the samples. For confirmation of the mesophase assignment, the glass substrates treated for either planar or homeotropic alignments were employed. Peak temperatures in the DSC traces due to phase transitions of the samples were found to be in agreement with those of the optical experiments. The transition temperatures obtained from calorimetric measurements of the first heating and cooling cycles at a rate of  $5\text{ }^\circ\text{C}/\text{min}$  are presented; in the cases where the signatures are not observed in DSC traces, the transition temperatures have been taken from the microscopic observations. The details of these studies with analysis of the results are presented in the following sections.

**II.b.1. Microscopic and Calorimetric Studies. DM-3,R Series.** The phase sequence, transition temperatures and the associated enthalpies of the DM-3,R series of compounds, in which the two rigid segments are separated by an 4-oxybutanoyloxy ( $C_4$ ; even-parity) spacer, are summarized in Table 1. As can be seen, all the compounds exhibit enantiotropic mesomorphism. Particularly, the lower homologues DM-3,6 and DM-3,7 show enantiotropic chiral nematic ( $N^*$ ) phase, the medium members DM-3,8, DM-3,9, DM-3,11, and DM-3,12, show enantiotropic  $N^*$ , twist grain boundary (TGB) and smectic A (SmA) phases, and the higher homologue DM-3,16 shows enantiotropic SmA phase only. This is in agreement with the fact that in many homologous series of calamitic LCs, the lower members are nematic, the medium members show nematic and smectic behavior, and the higher members are smectic only.<sup>1b,d</sup> However, these compounds display a rich transitional behavior during the cooling mode.

**Table 2.** Phase Transition Temperatures ( $^{\circ}\text{C}$ )<sup>c</sup> and Associated Enthalpies [ $\text{Jg}^{-1}$ ]<sup>d</sup> of Chiral Dimer-Like Compounds Belonging to the DM-4,R Series<sup>a</sup>

compound	phase sequence	
	heating	cooling
DM-4,6	Cr 99.5 [32.4] I	I 75.6 [32.3] Cr
DM-4,7	Cr 100.4 [50.1] I	I 76.3 [37.2] Cr
DM-4,8	Cr 100.7 [42.9] I	I 72.4 [32.7] Cr
DM-4,9	Cr 94.8 [26.6] Cr <sub>1</sub> 97.8 [11.4] I	I 75.3 [2.9] SmA 72.5 [24.8] Cr
DM-4,10 <sup>b</sup>	Cr 90 [39.1] I	I 76.9 [7.7] N* 64.1 [18.5] Cr
DM-4,11	Cr 78 [38.1] Cr <sub>1</sub> 81.3 [5] I	I 80.4 [5.1] SmA 68.6 <sup>e</sup> SmC* 62 <sup>f</sup> Cr
DM-4,12	Cr 65.5 [10.2] Cr <sub>1</sub> 78.2 [48.9] I	I 78.7 [9.3] SmA 72.4 <sup>e</sup> SmC* 63.5 <sup>f</sup> Cr
DM-4,16	Cr 75.2 [57.6] Cr <sub>1</sub> 81.5 [4.1] SmC* 83.7 [10.1] I	I 82.7 [10.1] SmC* 58.1 [29.2] Cr

<sup>a</sup> Cr = Cr<sub>1</sub> = crystal. <sup>b</sup> Known compound but included for the sake of comparison and completeness (ref 21). <sup>c</sup> Phase transition temperatures were determined by both POM and DSC studies: peak temperatures in the DSC thermograms obtained during the first heating and cooling cycles (at  $5\text{ }^{\circ}\text{C min}^{-1}$ ) coupled with optically measured temperatures are given. <sup>d</sup> Transition enthalpies were obtained from the DSC thermograms. <sup>e</sup> Phase transition was observed under POM; too weak to be detected by DSC. <sup>f</sup> Crystallization was observed under POM only.

For example, DM-3,6 stabilizes monotropic TGB and SmA phases, while DM-3,7 exhibits a metastable SmC\* phase additionally. The middle and the higher members stabilize a metastable SmC\* phase. The occurrence of SmC\*, SmA, TGB, and N\* phases was evidenced with the aid of polarizing microscope mainly.

A phase sequence, viz., N\*-TGB-SmA-SmC\* recognized for the compound DM-3,8, as a representative case, is discussed as follows. The sample was placed between a pair of ordinary glass slides, and upon cooling from its isotropic phase, the N\* phase appears with a focal conic texture that upon being subjected to mechanical stress yields a planar texture having oily streaks as shown in Figure 1a. Upon cooling further from the planar texture of the N\* phase, a transition to the TGB phase occurs where the oily streaks disappear to give a gray blurry planar texture (Figure 1b). On lowering the temperature further, the SmA phase appears with a characteristic focal-conic texture, as shown in Figure 1c. Of course, in some regions of the slide, a pseudoisotropic region typical of the SmA phase was observed. When this phase was cooled further, the SmC\* phase appears with a focal-conic fan texture featuring dechiralizaion lines (Figure 1d). The appearance of an arced equidistant line pattern superimposed on the fans indicates that the pitch of the helix of the phase is on the order of several micrometers. In the homeotropic regions, the SmC\* phase showed a cloudy greyish pattern, as expected. The TGB phase shows a typical filamentary textural pattern (Figure 1e) if it is obtained by heating the pseudoisotropic pattern of the SmA phase. Thus, the usage of ordinary slides made it possible to visualize the optical textural patterns arising due to both planar and homeotropic alignment of the molecules. Needless to mention, when slides treated for planar or homeotropic alignments were used, these mesophases showed the expected textural patterns. It is worth mentioning here that the above-mentioned phase sequences are highly

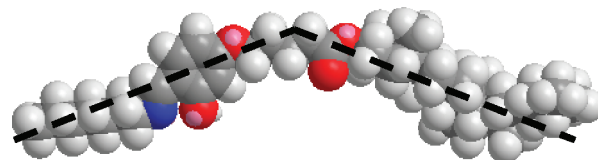


**Figure 3.** Energy minimized structures of dimer-like compound DM-4,7. Notice that the two cores are inclined with each other.

reproducible; as a representative case, the DSC traces obtained during the first and second heating/cooling scans are shown in Figure 2.

**DM-4,R Series.** Table 2 summarizes the thermal behavior of the DM-4,R series of dimer-like compounds. In this series, the cholesterol moiety and N-(n-alkyl)salicylaldimine core are tethered together through an 5-oxypentanoyloxy (odd-parity) spacer. It is immediately apparent from Table 2 that these compounds do not favor the mesomorphism convincingly. First three homologues DM-4,6, DM-4,7, and DM-4,8 are nonmesomorphic. The loss of mesomorphism in these compounds can be suitably interpreted in terms of pronounced bent molecular conformation (Figure 3) and thus, reduced shape anisotropy. The middle members DM-4,9, DM-4,11, and DM-4,12 exhibit monotropic LC behavior. More clearly, compound DM-4,9 displays the monotropic SmA phase; the SmA phase was identified based on the microscopic observation of a typical focal-conic texture using slides treated for planar orientation, and a dark field of view with slides treated for homeotropic orientation. The next two dimers, viz., DM-4,11 and DM-4,12, stabilize metastable SmA and SmC\* phases. These compounds placed between two glass slides treated for homeotropic orientation and cooled slowly from the isotropic liquid showed a pseudoisotropic pattern typical of the SmA phase. On cooling the sample further, the SmC\* phase appears with a cloudy texture. As expected, in slides treated for planar orientation, the SmA phase showed a focal-conic texture, whereas for the SmC\* phase dechiralization lines appear on the top of the focal-conic texture. Notably, the higher member DM-4,16 exhibits enantiotropic SmC\* phase. Subjecting the sample to planar boundary condition, the SmC\* phase from the isotropic phase appears as nucleating batonnets superimposed by the equidistant line pattern as shown in Figure 4a; on further cooling, the pattern fills the field of view. The DSC thermograms of the two heating and cooling cycles obtained for this compound are shown in Figure 4b; these traces corroborate the optical observation and also indicate the thermal stability of the compound.

**DM-5,R Series.** Table 3 gives the phase sequence, transition temperatures, and associated enthalpies for the compounds of the DM-5,R series wherein the cholesterol and N-(n-alkyl)-salicylaldimine moieties are connected through a 6-oxyhexanoyloxy (even-parity) spacer. Unlike the previous series of compounds, all the homologues exhibit enantiotropic mesomorphism. The first member DM-5,6 exhibits SmC\*, SmA, TGB, and N\* phases; of these, the SmC\* phase is metastable. The second homologue DM-5,7 stabilizes an identical phase sequence where only the N\* phase is enantiotropic in nature. The middle members DM-5,8–DM-5,12 exhibit enantiotropic SmA, TGB, and N\* mesophases in addition to a monotropic SmC\* phase. The higher member DM-5,16 displays an enantiotropic SmA phase in addition to a metastable SmC\* phase. Needless to say, all the mesophases were identified based on the observation of their

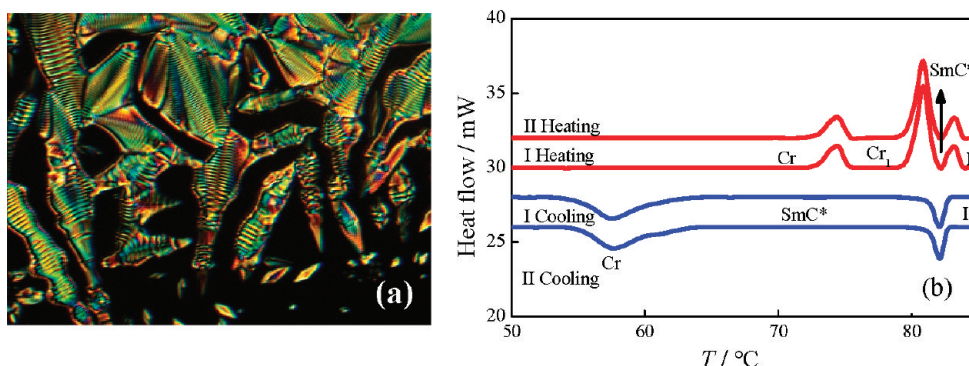


**Figure 4.** (a) Photomicrograph of the texture seen for the planar SmC\* phase appearing just below the isotropic phase of compound **DM-4,16**. (b) DSC traces of first and second heating/cooling cycles obtained for **DM-4,16** at a rate of  $5\text{ }^{\circ}\text{C min}^{-1}$ .

**Table 3. Phase Transition Temperatures ( $^{\circ}\text{C}$ )<sup>b</sup> and Associated Enthalpies [ $\text{Jg}^{-1}$ ]<sup>c</sup> of Chiral Dimer-like Mesogens of the DM-5,R Series**

Compound	Phase sequence	
	Heating	Cooling
<b>DM-5,6</b>	Cr 83.4 [40.3] SmA 92.4 TGB 93.4 [0.8] <sup>d</sup> N* 116.6 [2.8] I	I 116.2 [2.5] N* 92.9 TGB 90.8 [0.7] <sup>d</sup> SmA 44.4 <sup>e</sup> SmC*, <sup>f</sup>
<b>DM-5,7</b>	Cr 103.2 [68.4] N* 115.8 [3.5] I	I 115.3 [3.2] N* 99 TGB 97.3 [1.1] <sup>d</sup> SmA 63.3 <sup>e</sup> SmC*, <sup>f</sup>
<b>DM-5,8</b>	Cr 83.9 [48.4] SmA 96.5 TGB 101.5 [1.5] <sup>d</sup> N* 112.2 [3.2] I	I 111.7 [3.1] N* 101.2 TGB 95.2 [1.4] <sup>d</sup> SmA 66.9 <sup>e</sup> SmC*, <sup>f</sup>
<b>DM-5,9</b>	Cr 94.7 [55.5] SmA 102.1 TGB 104.3 [1.6] <sup>d</sup> N* 112.2 [4] I	I 111.7 [3.8] N* 103.9 TGB 101.8 [1.5] <sup>d</sup> SmA 78 <sup>e</sup> SmC*, <sup>f</sup>
<b>DM-5,10<sup>a</sup></b>	Cr 97.5 [53.6] SmA 103.3 TGB 104.9 [2] <sup>d</sup> N* 109.8 [3.9] I	I 109.3 [3.9] N* 104.6 TGB 102.9 [1.8] <sup>d</sup> SmA 81.1 <sup>e</sup> SmC*, <sup>f</sup>
<b>DM-5,11</b>	Cr 95.8 [52.1] SmA 104.8 TGB 106.5 [2] <sup>d</sup> N* 110 [4.6] I	I 109.3 [4] N* 106.1 TGB 104.6 [2] <sup>d</sup> SmA 86.5 <sup>e</sup> SmC* 29.8 Cr <sup>g</sup>
<b>DM-5,12</b>	Cr 93.4 [51.4] SmA 107.2 [1.8] N* 108.1 [3.4] I	I 107.5 [2.8] N* 106.6 [1.3] SmA 88.1 <sup>e</sup> SmC* 60.8 Cr <sup>g</sup>
<b>DM-5,16</b>	Cr 81.2 [39.4] SmA 106.6 [11.8] I	I 105.4 [11.8] SmA 79 <sup>e</sup> SmC* 51.8 Cr <sup>g</sup>

<sup>a</sup> Known compound but included for the sake of comparison and completeness (ref 21). <sup>b</sup> Phase transition temperatures were determined by both POM and DSC studies: peak temperatures in the DSC thermograms obtained during the first heating and cooling cycles (at  $5\text{ }^{\circ}\text{C min}^{-1}$ ) coupled with optically measured temperatures are given. <sup>c</sup> Transition enthalpies were obtained from the DSC thermograms. <sup>d</sup> Although N\*-TGB/TGB-N\* and TGB-SmA/SmA-TGB phase transitions were observed in POM, they were not resolved in the DSC trace. Hence the enthalpy value represents the combined enthalpy for N\*-TGB/TGB-N\* and TGB-SmA/SmA-TGB transitions. <sup>e</sup> Phase transition was observed under POM; too weak to be detected by DSC. <sup>f</sup> No crystallization was observed until the limitation of the DSC ( $-60\text{ }^{\circ}\text{C}$ ) instrument. <sup>g</sup> Crystallization was observed under POM only.

**Table 4. Phase Transition Temperatures ( $^{\circ}\text{C}$ )<sup>c</sup> and Associated Enthalpies [ $\text{Jg}^{-1}$ ]<sup>d</sup> of Chiral Dimer-Like Mesogens Belonging to the DM-7,R Series<sup>a</sup>**

Compounds	Phase sequence	
	Heating	Cooling
<b>DM-7,6</b>	Cr <sup>e</sup> 88.3 [32.6] N* 107.1 [3] I	I 106.3 [2.9] N* 72 <sup>f</sup> TGB 65.3 <sup>f</sup> SmA <sup>g</sup>
<b>DM-7,7</b>	Cr 95.5 [62.1] N* 106.1 [3.5] I	I 105.4 [3.4] N* 77.8 <sup>f</sup> TGB 53.7 <sup>f</sup> TGBC* -8.6 [3.8] M
<b>DM-7,8</b>	Cr 79.9 [50.4] SmA 83.9 TGB 87.2 [0.8] <sup>h</sup> N* 103.5 [3.4] I	I 103 [3.2] N* 86.6 TGB 82 [0.6] <sup>h</sup> SmA 61.1 <sup>f</sup> SmC* -7.1 [1.8] M
<b>DM-7,9</b>	Cr 89.1 [52.7] N* 102.6 [3.8] I	I 102.2 [3.8] N* 86 <sup>f</sup> TGB 84.5 <sup>f</sup> SmA 68.1 <sup>f</sup> SmC* -3.6 [2.3] M
<b>DM-7,10<sup>b</sup></b>	Cr 92.2 [55.9] N* 101 [3.9] I	I 100.6 [3.6] N* 91.4 <sup>f</sup> TGB 90 <sup>f</sup> SmA 72.9 <sup>f</sup> SmC* 14.6 [10.2] M
<b>DM-7,11</b>	Cr 85.2 [20.2] N* 95.6 [3] I	I 95.1 [2.7] N* <sup>e,f</sup>
<b>DM-7,12</b>	Cr 86.6 [47.6] SmA 93 TGB 94.1 [1.3] <sup>h</sup> N* 98.4 [4.4] I	I 97.6 [4.2] N* 93.5 TGB 92.8 [1.3] <sup>h</sup> SmA 78.7 <sup>f</sup> SmC* 41 [30.1] Cr
<b>DM-7,16</b>	Cr 74.2 [22.2] SmA 88.2 TGB 91.9 [0.6] <sup>h</sup> N* 94.3 [4.4] I	I 93.7 [3.8] N* 90.3 TGB 86.4[0.5] <sup>h</sup> SmA 72.4 <sup>f</sup> SmC* 49.4 [2.4] Cr

<sup>a</sup> TGBC\* = twist grain boundary phase with SmC\* blocks. <sup>b</sup> Known compound but included for the sake of comparison and completeness (see ref 21).

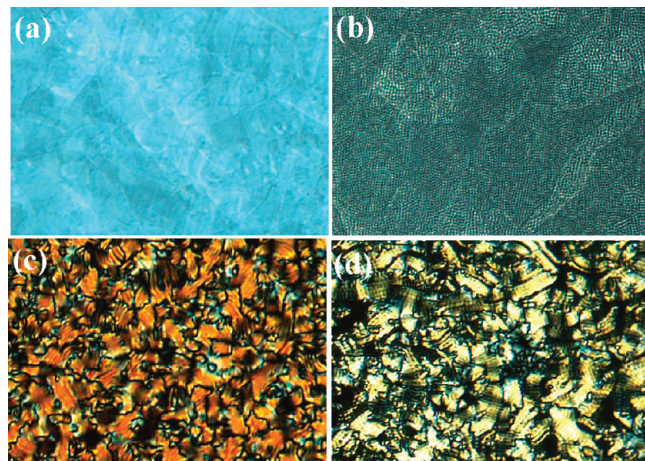
<sup>c</sup> Phase transition temperatures were determined by both POM and DSC studies: peak temperatures in the DSC thermograms obtained during the first heating and cooling cycles (at  $5\text{ }^{\circ}\text{C min}^{-1}$ ) coupled with optically measured temperatures are given. <sup>d</sup> Transition enthalpies were obtained from the DSC thermograms. <sup>e</sup> Crystal to crystal transition was observed for **DM-7,6** at 78.1 [12.5]. <sup>f</sup> Phase transition was observed under POM; too weak to be detected by DSC. <sup>g</sup> No crystallization was observed until the limitation of the DSC ( $-60\text{ }^{\circ}\text{C}$ ) instrument. <sup>h</sup> Although N\*-TGB/TGB-N\* and TGB-SmA/SmA-TGB phase transitions was observed in POM, it was not resolved in DSC trace. Hence the enthalpy value represents the combined enthalpy for N\*-TGB/TGB-N\* and TGB-SmA/SmA-TGB transitions.

characteristic textural patterns. For example, for compounds **DM-5,8–DM-5,12**, the microscopic examination revealed a

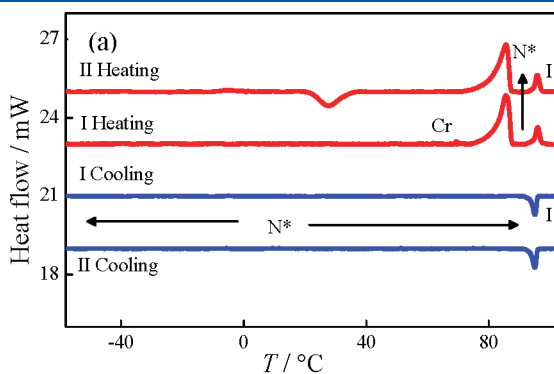
focal-conic texture for the N\* mesophase when untreated slides were used; indeed, the focal-conic texture changes into an oily

streak texture on slight shear. On further cooling, the  $N^*$  phase passes through a transient TGB phase to the SmA phase. The TGB phase showed a filament texture in the homeotropic alignment, as expected. The smectic A phase was recognized based on the observation of focal-conic texture in slides treated for planar orientation and a dark field of view in slides treated of homeotropic alignment. In slides treated for planar orientation the SmC\* phase shows dechiralization lines on top of the focal-conic fan texture, while with the surfaces treated for homeotropic alignment a cloudy texture was observed. It must be mentioned here that the phase transitions of all these compounds are highly reproducible for any number of heating and cooling cycles. The DSC thermograms of the first/subsequent heating and cooling scans corroborated the microscopic observations and further supported the repeatability of the transitions.

**DM-7,R Series.** The phase transitional behavior of the DM-7, R series of compounds is shown in Table 4. All the members of the series display enantiotropic mesomorphism. The first member DM-7,6 displays only  $N^*$  phase during heating, and while cooling it shows TGB and SmA phases additionally. The  $N^*$  phase showed characteristic focal-conic texture, which on slight

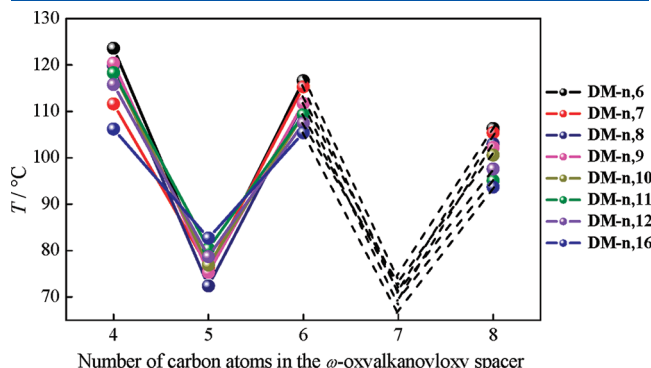


**Figure 5.** Photomicrographs of the textures of mesophase exhibited by compound DM-7,7: (a) planar texture of the TGB phase ( $72\text{ }^\circ\text{C}$ ), (b) square grid pattern of the TGBC\* phase emerging from the planar texture of the TGB phase ( $48\text{ }^\circ\text{C}$ ), (c) filamentary texture of the homeotropically aligned TGB phase ( $75\text{ }^\circ\text{C}$ ), and (d) undulated filamentary texture of the homeotropically aligned TGBC\* phase ( $48\text{ }^\circ\text{C}$ ).

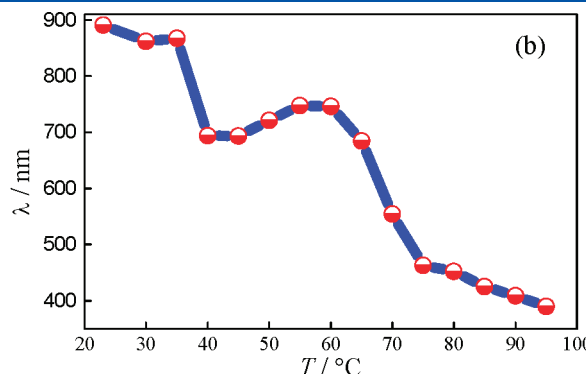


**Figure 6.** (a) DSC thermograms obtained during the first and second heating/cooling cycles at a rate of  $5\text{ }^\circ\text{C}/\text{min}$  for DM-7,11. Note that the  $N^*$  phase supercools well below the RT. (b) Plot showing the dependence of selective reflection wavelength of the  $N^*$  phase on the temperature of DM-7,11.

shearing gave Grandjean planar texture. For the TGB and SmA phases, planar/filamentary pattern and pseudoisotropic/focal-conic texture are observed when slides treated for homogeneous/homeotropic alignments were used. The second member DM-7,7 behaves almost identical to the first member except for the stabilization of the TGB phase having SmC\* blocks (denoted as the TGBC\* phase) additionally. Notably, the TGBC\* phase supercools until  $-8.6\text{ }^\circ\text{C}$ , at which it transforms into another unknown phase, hereafter referred to as the M phase as indicated by the DSC traces (see Table 4). The nature of the M phase could not be ascertained under POM owing to the temperature limitation of the hot-stage of our laboratory. On cooling the isotropic phase of compound DM-7,7, a focal-conic texture of the  $N^*$  phase appears sharply, which on mechanical shear furnishes a Grandjean planar texture. The planar texture of the  $N^*$  phase on further cooling transforms into a TGB phase (which may have either SmA or SmC blocks) as evidenced by the observation of a gray planar texture (Figure 5a). On lowering the temperature, a square grid pattern piercingly appears over the gray planar texture indicating the presence of a TGBC\* phase (Figure 5b). When the glass plates were treated to give a homeotropic alignment, filament pattern (Figure 5c) and an undulated filament texture (Figure 5d) were observed for the TGB and TGBC\* phase respectively. The next members DM-7,8 and DM-7,9 while cooling from the isotropic phase show an identical phase sequence:  $N^*$ –TGB–SmA–SmC\*–M where



**Figure 7.** The influence of the number of carbon atoms in the  $\omega$ -oxyalkoxy spacer on the clearing (isotropic liquid-mesophase) transition temperatures of four series of compounds. In all the plots, dashed lines joining points are suggestive of the general trend; it may be noted that experimental data do not cover for  $n = 7$ .



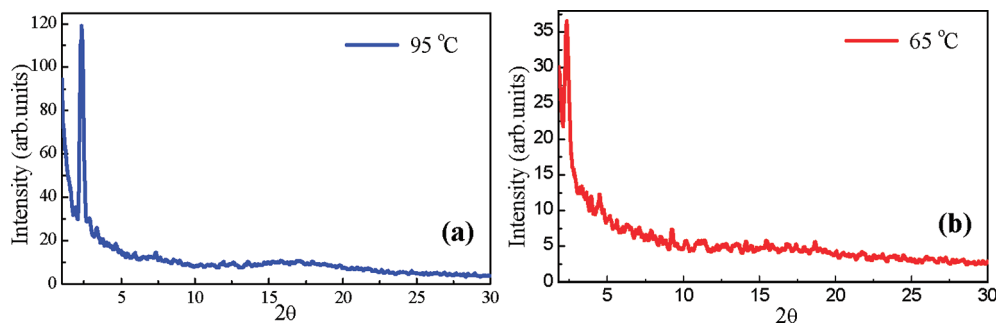


**Figure 8.** Intensity versus  $2\theta$  profile extracted from the 2D XRD pattern of the (a) SmA phase at  $95\text{ }^{\circ}\text{C}$  and (b) SmC\* phase at  $65\text{ }^{\circ}\text{C}$  of dimer-like compound DM-3,8.

**Table 5.** The Spacings ( $d_1$  and  $d_2$ ) Corresponding to the Low-Angle and Wide-Angle Reflections of XRD Pattern of Different Mesophases of Compounds DM-3,8, DM-5,10, and DM-7,6<sup>a</sup>

compound ( $L/\text{\AA}$ )	temperature / $^{\circ}\text{C}$	$d_1/\text{\AA}$ (intensity)	$d_2/\text{\AA}$ (intensity)	$d_1/L$	mesophase
DM-3,8 (38)	95	37.9 (s)	5.2 (d)	0.99	monolayer SmA (SmA <sub>1</sub> )
	65	34.8 (s)	5.1 (d)	0.91	SmC* (tilt angle = $23.3\text{ }^{\circ}$ )
DM-5,10 (45) <sup>b</sup>	90	43.9 (s)	5.1 (d)	0.98	SmA <sub>1</sub>
	75	39.2 (s)	5 (d)	0.87	SmC* (tilt angle = $30.9\text{ }^{\circ}$ )
DM-7,6 (42)	69	41.5 (s)	5.1 (d)	0.98	TGB with SmA <sub>1</sub> blocks
	60	41.2 (s)	5.1 (d)	0.98	SmA <sub>1</sub>

<sup>a</sup> The estimated all-trans molecular length ( $L$ ) and  $d_1/L$  ratio and structural assignment of the mesophases are also given. s: strong; d: diffuse. <sup>b</sup> Known compound; see ref 21.

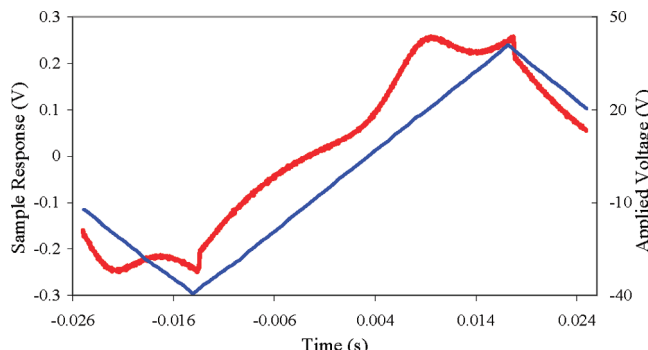


**Figure 9.** Current response peak obtained on application of a triangular wave field ( $\sim 8\text{ V}/\mu\text{m}$ ,  $16\text{ Hz}$ ) in the SmC\* phase of compound DM-3,16 at  $65\text{ }^{\circ}\text{C}$ . Note that the measured  $P_s$  is  $24\text{ nC cm}^{-2}$ .

M is an unknown phase existing well below room temperature (RT). A similar phase sequence but without the M phase was evidenced for the homologues DM-7,12 and DM-7,16.

Compound DM-7,11 stabilizes enantiotropic N\* phase solely, which is rather surprising given the observation that its immediate lower and higher members show a rich phase behavior. Notably, once the N\* phase formed upon melting of the sample, no sign of crystallization was noticed even after keeping the samples at RT for more than 6 days. However, repeated mechanical disturbances induced the phase to freeze in a glassy state. The DSC traces obtained (Figure 6a) corroborate the observation. Particularly, in the cooling cycle traces, only a signature due to the I-N\* phase is seen. The N\* phase showed vivid colors as the temperature was varied, indicating that the

pitch length of the N\* phase is on the order of the wavelength of incident visible light. The helical pitch is temperature-dependent and thus, the color of the reflected light varies with temperature, a feature that has been well used in temperature sensors. Thus, the temperature dependence of selective reflection was measured with the aid of ultraviolet-visible-near-infrared (UV-vis-NIR) scanning spectrophotometer coupled with a programmable hot stage. The sample DM-7,11 placed between two quartz plates was heated to its isotropic phase, and cooled slowly. The N\* phase formed was sheared to obtain Grandjean (planar) texture in which the helix of the phase becomes normal to the quartz plates and the structure reflects the incident light. After attaining this geometry, selective reflection wavelength as a function of temperature was recorded and during each scan, the temperature of the sample was kept constant. Figure 6b shows the thermal dependence of selective reflection ( $\lambda_{\max}$ ) in the entire thermal range (up to  $20\text{ }^{\circ}\text{C}$ ) of the N\* phase; a strong variation in the pitch with the variation in the temperature is apparent. The  $\lambda_{\max}$  shifts to longer wavelengths (redshift) as the temperature of the phase is lowered. However, as can be seen in Figure 6b, the pitch of the phase decreases and then increases in the temperature region between  $35$  and  $60\text{ }^{\circ}\text{C}$ , and this may be arising due to slow freezing of the N\* phase in the glassy state. Thus, the ability of this molecular design to change the pitch length and hence the N\* color over the visible region as a function of temperature is demonstrated.

The results of the thermal behavior of the four homologous series of dimer-like compounds formed by covalently linking cholesterol with *N*-(*n*-alkyl)salicylaldimine through either 4-oxybutanoyloxy or 5-oxypentanoyloxy or 6-oxyhexanoyloxy or 8-oxyoctanoyloxy spacer is surmised here. Within each series, the length of the flexible terminal tail varies from *n*-hexyl to

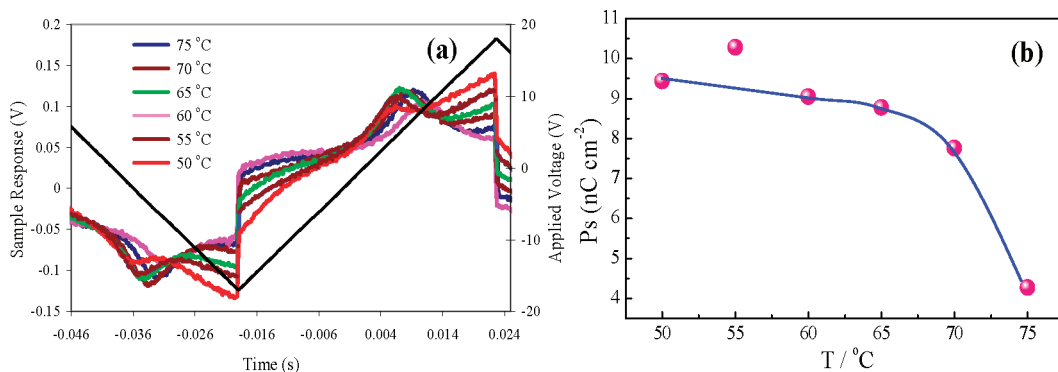


**Figure 10.** (a) Current response peaks obtained on application of a triangular wave field ( $5.04 \text{ V}/\mu\text{m}^{-1}$ , 12 Hz) in the  $\text{SmC}^*$  phase at different temperatures of compound **DM-5,10**. (b) The dependence of the  $P_s$  value on the temperature of the  $\text{SmC}^*$  phase of compound **DM-5,10**.

**Table 6. Electrochemical<sup>a</sup> Activities of Dimer-like Compounds**

compound	$E_{\text{OX}}^b$	$E_{\text{RED}}^b$	$E_{\text{HOMO}}^c$	$E_{\text{LUMO}}^c$	$\Delta E_{\text{CV}}^{c,d}$	$\Delta E_{\text{UV}}^{c,e}$
DM-3,6	1.20	-1.30	5.90	3.40	2.50	2.79
DM-3,8	1.21	-1.29	5.91	3.41	2.50	2.77
DM-3,16	1.19	-1.28	5.89	3.42	2.47	2.82
DM-5,7	1.15	-1.33	5.85	3.37	2.48	2.86
DM-5,9	1.14	-1.29	5.84	3.41	2.43	2.92
DM-5,10	1.19	-1.24	5.89	3.46	2.43	2.90
DM-7,6	1.14	-1.30	5.84	3.40	2.44	2.85
DM-7,8	1.19	-1.23	5.89	3.47	2.42	2.85
DM-7,10	1.19	-1.27	5.89	3.43	2.46	2.84
DM-7,11	1.14	-1.29	5.84	3.41	2.43	2.83

<sup>a</sup> Experimental conditions: Pt-disk working electrode, Pt-wire counter electrode,  $\text{Ag}/\text{Ag}^+\text{Cl}^-$  in saturated LiCl solution as reference electrode,  $(\text{Bu})_4\text{NPF}_6$  (0.1 M), RT. <sup>b</sup> In volts (V). <sup>c</sup> In electron volts (eV). <sup>d</sup> Estimated band gap from the onset oxidation and reduction potential (vs  $\text{Ag}/\text{Ag}^+$ ) plus 4.7 (see refs 27d and 27e). <sup>e</sup> Band gap determined from the red edge of the longest wavelength in the UV-vis absorption of compounds.

*n*-dodecyl and *n*-hexadecyl, whereas the nature of the spacer obviously remained unaltered. Within each series, the variation of the length of the terminal tail seems to influence the phase transitional behavior. In some of the series, a general trend seems to be followed, especially during the heating cycle, where the lower members are chiral nematics ( $\text{N}^*$ ), the medium members show chiral nematic and smectic (SmA and  $\text{SmC}^*$ ) behavior with frustrated phases (TGB), and the higher members are smectics. In each series, the clearing temperature decreases with the increase in the terminal tail length. In comparison with an even-parity spacer containing three series of compounds, the homologous series comprising an odd-parity spacer show lower clearing temperatures, as summarized in Figure 7; such a behavior can be explained in terms of their overall molecular shape governed by the geometry and flexibility of the spacer.

*II.b.2. XRD Study.* As discussed in a recent review article,<sup>5d</sup> the SmA phase formed by the cholesterol-based dimer, shows fascinating structural variations (periodicities) that largely depend upon the relative lengths of the spacer and terminal chains as well as, to an extent, the nature of the aromatic core. For example, the monolayer or partially bilayered SmA phase is seen if the spacer length is less than the length of the terminal tail. The intercalated SmA phase is stabilized if the spacer is longer than the terminal chain and the smectic phase disappears when the

two lengths are comparable.<sup>5d</sup> Therefore, it is interesting to examine whether the structure of the SmA phase is governed by the relative lengths of spacer and terminal tail in these cholesterol-based dimer-like compounds. XRD study was carried out on **DM-3,8** and **DM-7,6** as representative cases; for the comparison, the known compound **DM-5,10**<sup>21</sup> was also investigated. These samples were individually filled in a Lindemann capillary (1 mm diameter) tube in the isotropic phase, and both the ends of the tube were flame-sealed. The diffraction patterns obtained as a function of temperature in different mesophases were collected in the cooling mode. The XRD patterns obtained for the mesophases were found to be nearly identical; they consisted of a diffuse peak and a sharp peak in the wide angle and low angle regions, respectively. As a representative case, the 1D intensity versus  $2\theta$  profiles derived from two-dimensional (2D) XRD patterns of the SmA and  $\text{SmC}^*$  phases of **DM-3,8** are shown in Figure 8. The spacings ( $d_1$ ) derived from the low angle Bragg reflections of the mesophases in each compound are indicative of the layered structure. The measured spacings ( $d_2$ ) of wide angle diffuse reflections correspond to liquid-like order within the layers. These spacings and the ratio  $d_1/L$ , where  $L$  is the estimated all-*trans* molecular length derived from a Chem3D molecular model, are presented in Table 5.

As can be seen in Table 5, the  $d_1$ -values obtained for the SmA phases of dimer-like compounds **DM-3,8**, **DM-5,10**, and **DM-7,6** are 37.9, 43.9, and 41.5 Å, respectively; in fact, these values are nearly equivalent to the estimated all-*trans* molecular lengths 38, 45, and 42 Å for **DM-3,8**, **DM-5,10**, and **DM-7,6**, respectively. Thus, the  $d_1/L$  ratio is one suggesting the monolayered arrangement of molecules in the SmA phase. The formation of monolayer SmA (SmA<sub>1</sub>) phase by **DM-3,8** and **DM-5,10** is in agreement with the general observation that the cholesterol-based dimers<sup>5d</sup> having the spacer length less than the length of the terminal tail stabilize SmA<sub>1</sub> phase. The collected data in the  $\text{SmC}^*$  phase for **DM-3,8** and **DM-5,10** reveals that the layer spacing  $d_1$  is much less than the molecular length  $L$ , and thus the  $d_1/L$  ratio is less than 1. This is expected considering the fact that in the  $\text{SmC}^*$  phase, the molecules tilt with respect to the layer normal direction.

*II.b.3. Electrical Switching Studies.* It may be reiterated here that, except for a few, all the dimer-like compounds synthesized stabilize the  $\text{SmC}^*$  phase; notably, in the majority of the cases, it exists over a fairly wide thermal range. Most importantly, the electric switching behavior of the phase is known to be useful in fabricating display devices.<sup>1</sup> Thus, the  $\text{SmC}^*$  phase of these

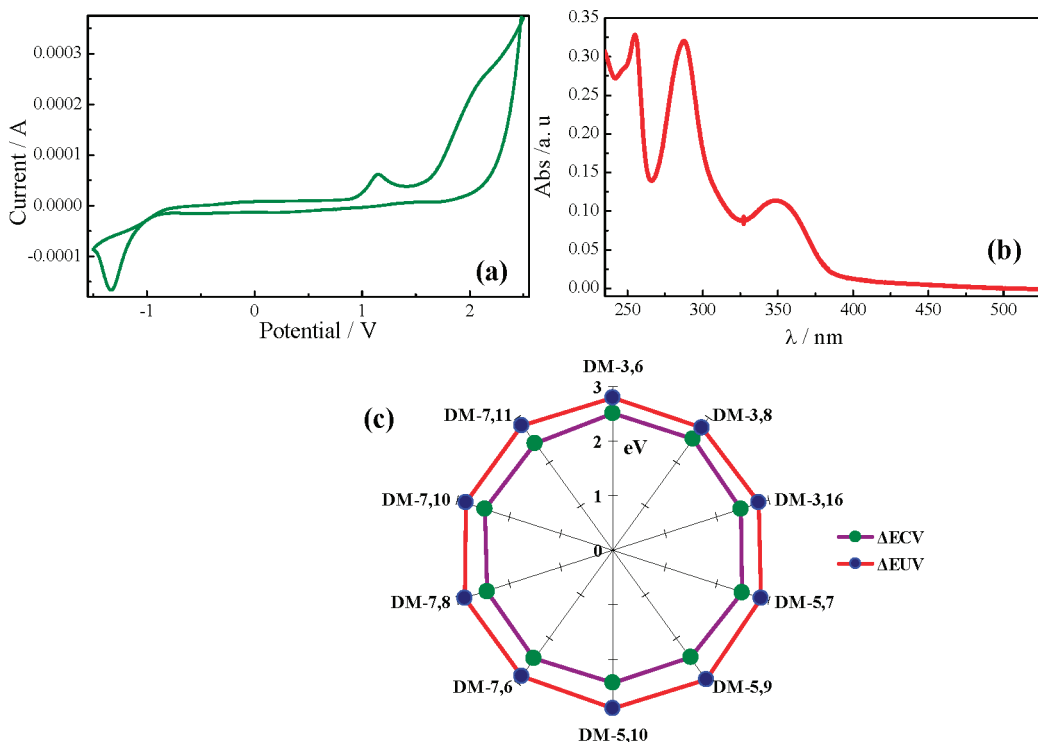


**Figure 11.** (a) Cyclic voltammogram of **DM-5,7** ( $10^{-3}$  M/CH<sub>2</sub>Cl<sub>2</sub>) at a scan rate of 100 mVs<sup>-1</sup>. (b) UV absorption spectrum ( $10^{-3}$  M/CH<sub>2</sub>Cl<sub>2</sub>) obtained for **DM-5,7**. (c) Energy gaps expressed in electron volts deduced by both CV and UV experiments.

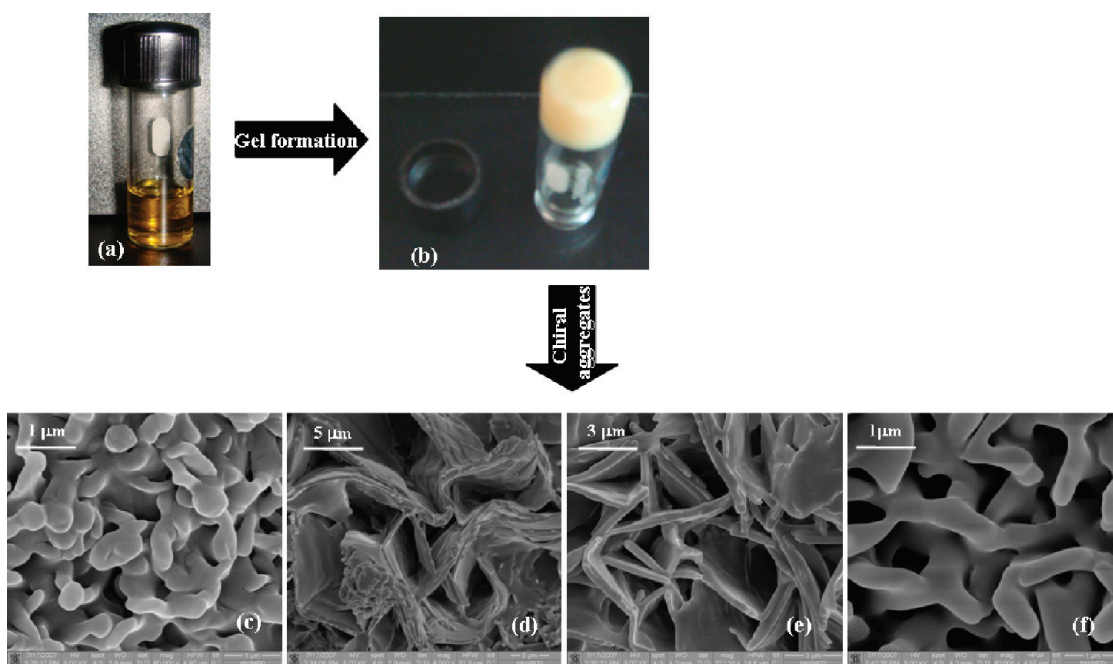


**Figure 12.** (a) Vial comprising a hot clear solution of **DM-7,16** in 2% (w/v) ethanol. (b) Vial is inverted to show the formation of stable gel at RT. Also shown are the SEM images (c–f) of **DM-7,16** gel in 2% ethanol having different morphologies of micrometer size.

dimer-like compounds was investigated for its switching property, and the study revealed their ferroelectric switching behavior. For the purpose of this study, cells (5.01  $\mu$ m thick) were built using indium tin oxide (ITO)-coated glass plates pretreated with a polyimide solution, which enables the molecules to align

homogeneously. The samples in their isotropic phase were filled into the cell by capillary action and cooled slowly. After attaining the SmC\* phase, a triangular-wave field was applied where the samples showed the current response curves. As a representative case, the current response profile obtained for **DM-3,16**

on application of a low frequency (16 Hz) triangular-wave field ( $\sim 8 \text{ V}/\mu\text{m}$ ) at 65 °C is illustrated in Figure 9. As can be seen, the current passing through the sample shows one peak per half period of the applied field, indicating the ferroelectric behavior of the SmC\* phase. The area under the peak trace is a direct measure of  $P_s$  and it was found to be 24 nC cm<sup>-2</sup>. Seemingly, the  $P_s$  value is small but increases upon lowering the temperature, as expected. In some cases, the value of  $P_s$  was found to be much smaller; this is especially notable in one of four known compounds, **DM-5,10** studied. Figure 10a illustrates the electrical response profiles obtained on applying a triangular wave electrical field of 5 V  $\mu\text{m}^{-1}$  (12 Hz) at different temperatures of the SmC\* phase. The temperature dependence of  $P_s$  obtained by integrating the area under the peaks is shown in Figure 10b. It can be seen that the  $P_s$  value is quite small but increases with the decrease in temperature, as expected. The smaller magnitude of spontaneous polarization found in these compound can be attributed to the weak intramolecular transfer of the bulky chirality from the cholesterol unit to the other mesogens.

### III. ELECTROCHEMICAL BEHAVIOR

In recent times, cholesterol-based oligomesogens have been shown to be multifunctional.<sup>23–25</sup> For example, their antimicrobial activity<sup>23</sup> and electrochemical behavior<sup>24,25</sup> have been revealed recently. Inspired by these findings, we intended to probe these synthesized dimer-like compounds for their electrochemical behavior. Thus, the oxidation–reduction potentials were measured by cyclic voltammetry (CV) at a scanning rate of 100 mV s<sup>-1</sup> for the millimolar solutions of several randomly selected compounds in dichloromethane;<sup>26</sup> the results deduced from this study are summarized in Table 6. Tetrabutylammonium hexafluorophosphate (0.1 M) in dichloromethane was used as a supporting electrolyte (buffer). A conventional three-electrode cell, consisting of a 1 mm diameter platinum disk as a working electrode, silver–silver chloride as a reference electrode, and a platinum wire as a counter electrode, were used. The reference electrode consisted of a Ag/Ag<sup>+</sup>Cl<sup>-</sup> electrolyte in saturated lithium chloride solution. The electrochemical potential was calibrated with respect to a ferrocene/ferrocenium (Fc/Fc<sup>+</sup>) couple. As a representative case, the cyclic voltammogram obtained for the compound **DM-5,7** is shown in Figure 11a. The IP ( $E_{\text{HOMO}}$ ) and EA ( $E_{\text{LUMO}}$ ) were determined by adding 4.7 eV (vs Ag/Ag<sup>+</sup>Cl<sup>-</sup>) to the first oxidation and first reduction potentials, respectively, and the difference between these furnished the energy gaps ( $\Delta E_{\text{CV}}$ ).<sup>26,27</sup> The energy gap ( $\Delta E_{\text{UV}}$ ) was also deduced from the red edge of the longest wavelength absorption (Figure 11b), using the expression  $E = h\nu$  (where  $\nu = c/\lambda$ ). Seemingly,  $\Delta E$  values deduced from both the methods are nearly comparable, indicating that these compounds genuinely possess electrochemical activity. The schematic representation of energy gap deduced by both CV and UV experiments is shown in the Figure 11c.

### IV. GELATION STUDY

Gels derived from low molecular mass compounds have been attracting a great deal of attention as they hold promise for a number of biological and materials applications.<sup>28,29</sup> This is especially notable in the case of compounds/mesogens (gelators) derived from cholesterol as they form stable organic gels that have been regarded as novel molecular recognition systems,

sensing and external stimuli responsive motifs, light harvesting systems, templates for the transcription of nanofibrous materials, and so forth.<sup>28,29</sup> Given the fact that the synthesized dimer-like molecules possess a cholesterol component, we became interested in examining their gelation ability and the morphology of the gel formed. Thus, a qualitative investigation on the gelation ability of all the synthesized dimer-like compounds was carried out. A series of common organic solvents were employed to reveal the gelation behavior of the compounds. Our study shows that these compounds readily dissolve in dichloromethane, chloroform, diethylether, and tetrahydrofuran but are insoluble in hexanes as well as in protic solvents such as methanol and ethanol. However, these compounds were found to be soluble in hot ethanol and reappear upon cooling in the form of soft mass, indicating their ability to gelatinize. Thus, the minimum gelation concentration (MGC) necessary for gel formation in ethanol was investigated; the study revealed the formation of gel with an MGC of 2 g/100 mL. For example, a mixture of **DM-7,16** (20 mg) and absolute ethanol (1 mL) was warmed in a screw-capped vial until the compound dissolved (Figure 12a). The homogeneous solution thus formed was cooled to RT yielding gel; this was ascertained by the test tube inversion method as illustrated in Figure 12b. Of course, the sol to gel phase was found to be thermally reversible. A scanning electron microscope (SEM) was used to evaluate the gel morphology. The SEM images obtained are illustrated in Figures 12c–f. These images indicate the self-assembly of these chiral molecules into different morphologies at a supramolecular scale of micrometer size.

### V. SUMMARY

It is demonstrated that the thermal behavior and other functional characteristics of a relatively new class LCs, called dimer-like mesogens, are similar to that of well-known LC dimers. Thereby, the synthesis and various properties characterization of 28 new optically active dimer-like compounds belonging to four series are reported. They are made by covalently tethering cholesterol with a salicylideneamine core through an  $\omega$ -oxyalkanoyloxy spacer of varying length and parity. These four series of compounds primarily differ in the number of carbon atoms (length and parity) of the spacer. With a few exceptions in the series having odd-parity spacers, all the compounds exhibit enantiotropic mesomorphism. In all the three even-parity spacer series, the variation in the length of the terminal tail influences the thermal property. For example, the lower members display the N\* phase, the medium members show the N\* and smectic phases intervened by the TGB phase, and the higher members are purely smectics. Notably, in some cases, the N\* and SmC\* phases exist over a wide thermal range; the latter phase exhibits ferroelectric switching behavior. A dramatic odd–even effect in the clearing temperatures occurs wherein the even-parity dimers possess higher values. Thus, the thermal behavior of these dimer-like compounds is analogous to that of LC dimers. Most importantly, this study has demonstrated that the terminal phenyl ring of dimer-like compounds should have an *n*-alky tail to stabilize thermodynamically stable mesophases. UV–vis study demonstrated the temperature dependences of the wavelength selective reflection ( $\lambda_{\text{max}}$ ) of the phase. The redox behavior of some representative samples has been probed by CV experiments, and the energy gaps are estimated by both CV and UV experiments. The results of these measurements are comparable, which emphasize that they genuinely possess electrochemical

activity. Notably, these compounds have the tendency to form stable organic gel in ethanol where the gelators self-assemble into chiral aggregates with different morphologies of micrometer size.

## ■ ASSOCIATED CONTENT

**5 Supporting Information.** Detailed experimental procedures and molecular characterization data. This information is available free of charge via the Internet at <http://pubs.acs.org>

## ■ AUTHOR INFORMATION

### Corresponding Author

\*Tel: 91-80-28381119. Fax: 91-80-28382044. E-mail: yelamaggad@csmr.res.in or yelamaggad@gmail.com.

### Present Addresses

<sup>†</sup>Institute of Chemistry, Organic Chemistry, Martin-Luther-University, Halle-Wittenberg, Kurt Mothes Str. 2, D-06120 Halle/Saale, Germany.

## ■ ACKNOWLEDGMENT

The authors express their gratitude to Dr. D. S. Shankar Rao for providing the X-ray diffraction data. Dr. S. Krishna Prasad is gratefully acknowledged for helpful discussions. The authors wish to thank Ms. Sandhya D. Hombal (CSMR) for her technical assistance; Dr. Gurumurthy Hegde for helping in carrying out electrical switching experiments; Dr. M. Pandurangappa and Mr. T. Ramakrishnappa, Central College, Bangalore, for their help in carrying out cyclic voltammetry experiments; and Prof. G. U. Kulkarni, JNCSR, for providing SEM images.

## ■ REFERENCES

- (a) Chandrasekhar, S. *Liquid Crystals*, 2nd ed.; Cambridge University Press: Cambridge, U.K., 1994. (b) Collings, P. J.; Hird, M. *Introduction to Liquid Crystals Chemistry and Physics*; Taylor and Francis Ltd.: London, 1997. (c) Bahadur, B. *Liquid Crystals: Application and Uses*; World Scientific: Singapore, 1990; Vols. 1–3. (d) Goodby, J. W. In *Hand Book of Liquid Crystals*; Demus, D., Goodby, J. W., Gray, G. W., Spiess, H.-W., Eds.; Wiley-VCH: Weinheim/New York, 1998; Vol. I. (e) Kitzerow, H. In *Chirality in Liquid Crystals*; Kitzerow, H.-S., Bahr, C., Eds.; Springer-Verlag, Inc.: New York, 2001.
- Goodby, J. W.; Saez, I. M.; Cowling, S. J.; Gortz, V.; Draper, M.; Hall, A. W.; Sia, S.; Cosquer, G.; Lee, S.-E.; Peter Raynes, E. *Angew. Chem., Int. Ed.* **2008**, *47*, 2754–2787.
- (a) Demus, D. *Liq. Cryst.* **1989**, *5*, 75–110. (b) Tschierske, C. *J. Mater. Chem.* **1998**, *8*, 1485–1508. (c) Tschierske, C. *J. Mater. Chem.* **2001**, *11*, 2647–2671. (d) Tschierske, C. *Annu. Rep. Prog. Chem., Sect. C* **2001**, *97*, 191–267. (e) Tschierske, C. *Curr. Opin. Colloid Interface Sci.* **2002**, *7*, 69–80.
- Imrie, C. T.; Henderson, P. A. *Chem. Soc. Rev.* **2007**, *36*, 2096–2124.
- (a) Imrie, C. T.; Luckhurst, G. R. In *Handbook of Liquid Crystals*; Demus, D., Goodby, J. W., Gray, G. W., Spiess, H.-W., Vill, V., Eds.; Wiley-VCH: Weinheim, Germany, 1998; Vol. 2B. (b) Imrie, C. T.; Henderson, P. A. *Curr. Opin. Colloid Interface Sci.* **2002**, *7*, 298–311. (c) Imrie, C. T. In *Structure and Bonding - Liquid crystals, II*; Mingos, D. M. P., Ed.; Springer-Verlag: New York, 1999; p 149. (d) Yelamaggad, C. V.; Shanker, G.; Hiremath, U. S.; Krishna Prasad, S. *J. Mater. Chem.* **2008**, *18*, 2927–2949.
- (a) Hardouin, F.; Achard, M. F.; Jin, J.-I.; Shin, J.-W.; Yun, Y. K. *J. Phys. II* **1994**, *4*, 627–643. (b) Hardouin, F.; Achard, M. F.; Jin, J.-I.; Yun, Y. K. *J. Phys. II* **1995**, *5*, 927–935. (c) Cha, S.-W.; Jin, J.-I.; Achard, M. F.; Hardouin, F. *Liq. Cryst.* **2002**, *29*, 755–763. (d) Lee, J.-W.; Park, Y.; Jin, J.-I.; Achard, M. F.; Hardouin, F. *J. Mater. Chem.* **2003**, *13*, 1367–1372. (e) Kim, K.-N.; Do, E.-D.; Kwon, Y.-W.; Jin, J.-I. *Liq. Cryst.* **2005**, *32*, 229–237.
- Gray, G. W.; Harrison, K. *J. Mol. Cryst. Liq. Cryst.* **1971**, *13*, 37–60.
- Gray, G. W.; Harrison, K. *Symp. Faraday Soc.* **1971**, *5*, 54–67.
- Gray, G. W. *J. Phys. (Paris)* **1975**, *36*, 337–347.
- Coates, D.; Gray, G. W. *J. Phys. (Paris)* **1975**, *36*, 365–370.
- (a) Ennulat, R. D.; Brown, A. J. *Mol. Cryst. Liq. Cryst.* **1971**, *12*, 367–378. (b) Ennulat, R. D.; Brown, A. J. *Mol. Cryst. Liq. Cryst.* **1969**, *8*, 247–265.
- (a) Elser, W.; Pohlman, J. L. W.; Boyd, P. R. *Mol. Cryst. Liq. Cryst.* **1971**, *15*, 175–182. (b) Sisndo, M.; Takeuchi, K.; Imanishi, Y. *J. Phys. Chem.* **1984**, *88*, 2893–2898. (c) Koden, M. K.; Miyake, S.; Takenaka, S.; Kusabayash, S. *J. Phys. Chem.* **1984**, *88*, 2387–2390. (d) Pohlman, J. L. W.; Elser, W.; Boyd, P. R. *Mol. Cryst. Liq. Cryst.* **1973**, *20*, 87.
- Marcelis, A. T. M.; Koudijs, A.; Sudholter, E. J. R. *Liq. Cryst.* **1995**, *18*, 843–850.
- Itahara, T. *Liq. Cryst.* **2005**, *32*, 115–118.
- Berardi, R.; Muccioli, L.; Zannoni, C. *ChemPhysChem* **2004**, *5*, 104–111.
- Cowling, S. J.; Hall, A. W.; Goodby, J. W. *Liq. Cryst.* **2005**, *32*, 1483–1498.
- Cowling, S. J.; Hall, A. W.; Goodby, J. W. *Chem. Commun.* **2005**, 1546–1548.
- Cowling, S. J.; Hall, A. W.; Goodby, J. W. *Adv. Mater.* **2005**, *17*, 1077–1080.
- Cowling, S. J.; Hall, A. W.; Goodby, J. W. *Chem. Commun.* **2006**, 4107–4109.
- Dodge, M. R.; Vij, J. K.; Cowling, S. J.; Hall, A. W.; Goodby, J. W. *Liq. Cryst.* **2005**, *32*, 1045–1051.
- Yelamaggad, C. V.; Rashmi, Prabhu; Shanker, G.; Bruce, D. W. *Liq. Cryst.* **2009**, *36*, 247–255.
- (a) Mukkamala, R.; Weiss, R. G. *Langmuir* **1996**, *12*, 1474–1482. (b) Surendranath, V. *Mol. Cryst. Liq. Cryst.* **1999**, *332*, 135–140. (c) Hamley, I. W.; Castelletto, V.; Parras, P.; Lu, Z. B.; Imrie, C. T.; Itoh, T. *Soft Matter* **2005**, *1*, 355–363.
- Yelamaggad, C. V.; Shanker, G. *Tetrahedron* **2008**, *64*, 3760–3711.
- Yelamaggad, C. V.; Achalkumar, A. S.; Shankar Rao, D. S.; Krishna Prasad, S. *Org. Lett.* **2007**, *9*, 2641–2644.
- Yelamaggad, C. V.; Shanker, G. *Liq. Cryst.* **2007**, *34*, 1045–1057.
- Lundia, N. J.; Blackman, A. G.; Gordon, K. C.; Officer, D. L. *Angew. Chem., Int. Ed.* **2006**, *45*, 2582–2584.
- (a) Li, Y.; Cao, Y.; Gao, J.; Wang, D.; Yu, G.; Heeger, A. J. *Synth. Met.* **1999**, *99*, 243–248. (b) de Leeuw, D. M.; Simenon, M. M. J.; Brown, A. R.; Einerhand, R. E. F. *Synth. Met.* **1999**, *87*, 53–59. (c) Cui, Y.; Zhang, X.; Jenekhe, S. A. *Macromolecules* **1999**, *32*, 3824–3826. (d) Wang, H.-Yu.; Feng, J.-C.; Wen, G.-An.; Jiang, H.-J.; Wan, J.-H.; Zhu, R.; Wang, C.-M.; Wei, W.; Huang, W. *New J. Chem.* **2006**, *30*, 667–670. (e) Jiang, J.; Shen, Z.; Lu, J.; Fu, P.; Lin, Y.; Tang, H.; Gu, H.; Sun, J.; Xie, P.; Zhang, R. *Adv. Mater.* **2004**, *16*, 1534–1558. (f) Kittel, C. *Introduction to Solid State Physics*, 7th ed.; John Wiley & Sons, Inc.: Singapore/New York, 1995; p 201. (g) Wang, X.-H. M.; Lei, S.-B.; Yang, Y.-L.; Wang, C. J. *Mater. Chem.* **2006**, *16*, 4265–4269. (h) Mishra, S. P.; Krishnamoorthy, K.; Sahoo, R.; Kumar, A. *J. Mater. Chem.* **2006**, *16*, 3297–3304. (i) Sotomura, T.; Uemachi, H.; Takeyama, K.; Naoi, K.; Oyama, N. *Electrochim. Acta* **1992**, *37*, 1851–1854.
- (a) Terech, P.; Weiss, R. G. *Chem. Rev.* **1997**, *97*, 3133–3159. (b) Sangeetha, N. M.; Maitra, U. *Chem. Soc. Rev.* **2005**, *34*, 821–836. (c) Banerjee, S.; Das, R. K.; Maitra, U. *J. Mater. Chem.* **2009**, *19*, 6649–6687.
- Shinkai, S.; Murata, K. *J. Mater. Chem.* **1998**, *8*, 485–495 and references cited therein.